Letter

Experimental measurement of quantum first-passage time distributions

Joseph M. Ryan, * Simon Gorbaty, Thomas J. Kessler, Mitchell G. Peaks, Stephen W. Teitsworth, and Crystal Noel
Duke Quantum Center, Department of Electrical and Computer Engineering and Department of Physics, Duke University, Durham, North Carolina 27708, USA

(Received 8 September 2025; revised 13 January 2026; accepted 1 April 2026; published 7 May 2026)

Classical first-passage time distributions have been extensively studied both theoretically and experimentally. Their quantum counterparts—quantum first-passage time distributions (QFPTDs)—remain largely unexplored and have deep implications for both fundamental physics and the development of emerging quantum technologies. We measure the first QFPTDs using a motional mode of a single trapped ion. We develop a composite-phase laser pulse sequence to perform tunable stroboscopic single-shot projective measurements of the motional state of a trapped ion. We measure QFPTDs of the ion energy when coupled to electric-field noise. The measurement protocol developed here is broadly applicable to other quantum systems and provides a powerful method for exploring a broad range of QFPTD phenomena. With these results, we open a field of experimental investigations of QFPT processes with potential future relevance to quantum search algorithms, unraveling connections between classical and quantum dynamics, and study of the quantum measurement problem.

DOI: 10.1103/p3pl-1m6n

Introduction. The first-passage time is typically defined as the first time that a system dynamical observable is measured to be outside a *surviving domain*. Distributions of these times, known as First-Passage Time Distributions (FPTDs), have a long history in science. They reveal individual trajectory dynamics that ensemble quantities may fail to capture [1–3], as exemplified by Schrödinger's clarification of Millikan's oil drop experiment [4]. FPTDs have since been used in diverse areas such as in the study of activation in chemical and biological processes [3,5–8], current switching in electronic transport structures [9,10], economics and market models [11–14], and climate science [15–17].

There are important differences between the classical and the quantum FPTD problem. In the classical case, FPTDs are only defined for stochastic processes. A deterministic process would have a delta-function FPTD. However, in the quantum case, measurements themselves introduce randomness. Thus, even a unitarily evolving quantum system with interspersed measurements has a nontrivial distribution of first-passage times. In this Letter, we focus on the quantized motion of a harmonic oscillator driven by additive noise, although the measurement protocol developed here can be used for any other time evolution. The first-passage time is defined as the earliest time at which the ion is *measured* to have an energy greater than or equal to a certain barrier $E_B = \hbar\omega(N_B + \frac{1}{2})$, after initialization in the ground state $|0\rangle$ and under projective measurements performed at fixed intervals θ. Figure 1 presents sample trajectories (generated using the Monte Carlo wavefunction method [18]) in the energy basis that illustrate key conceptual differences between quantum and classical descriptions of this problem. In particular, a quantum trajectory can be in a superposition of states both inside and outside the surviving domain, in which case a measurement alters the wavefunction—a fundamentally quantum effect. In the case that the measurement results in survival, the energy of the trajectory is decreased. Furthermore, a trajectory whose mean energy is less than the barrier energy may still be detected as having escaped the surviving domain. In this model, the noisy diffusion along the energy ladder is caused by both the additive noise and the quantum projective measurement. Additional quantum properties such as the (anti-)Zeno effect [19] make general Quantum First-Passage Time Distributions (QFPTDs) richer than their classical counterpart and place them at the interface of quantum and classical mechanics. We note that the classical analog of this problem is both nontrivial and subtle due to the multidimensional boundary condition [20].

Measurements at regular intervals (stroboscopic) have become an accepted method of interpreting the problem of QFPTDs [21], although measurements at random intervals [22] and continuous measurements of open quantum systems [23] have also been investigated. Since time is not a self-adjoint operator, QFPTDs are ambiguously defined in the continuous measurement limit [24–26]. This ambiguity highlights the need for experimental validation of newly obtained theoretical results—among them, the exotic predictions of spin-dependent arrival times [27–29].

Quantum walk search algorithms [30–34] are naturally understood as quantum first-passage processes [21–24,35–45]. The development of experimental QFPTD methods has potential to further our understanding of these analytically challenging algorithms with known exponential speedup and

*Contact author: joseph.ryan@duke.edu

Published by the American Physical Society under the terms of the Creative Commons Attribution 4.0 International license. Further distribution of this work must maintain attribution to the author(s) and the published article's title, journal citation, and DOI.

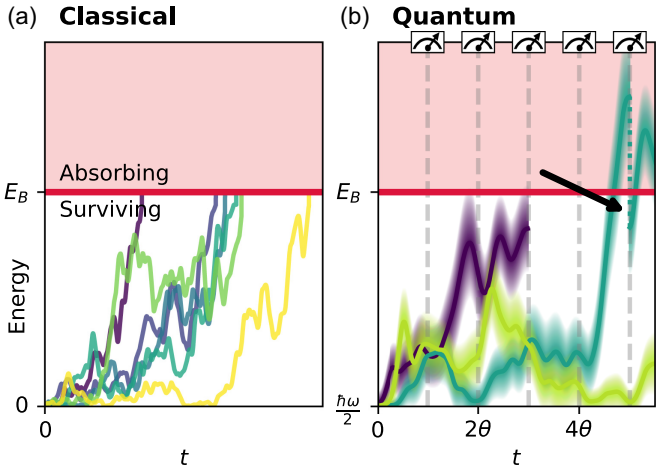


FIG. 1. Conceptual comparison of quantum and classical FPTs with energy threshold E_B. (a) Sample classical FPT trajectories with continuous measurement, which end when the energy is greater than E_B. In contrast to their quantum counterpart, they can start with zero initial energy. (b) Sample quantum trajectories, starting in $|0\rangle$, under stroboscopic projective measurement at increment θ. The trajectories are superpositions of energy eigenstates whose mean energy is shown with a solid line and whose standard deviation is represented by the shading. Note that the trajectory indicated by the arrow has an average energy larger than E_B, but the measurement at $t = 5\theta$ results in *survival* and the wavefunction is projected back into the *surviving domain*.

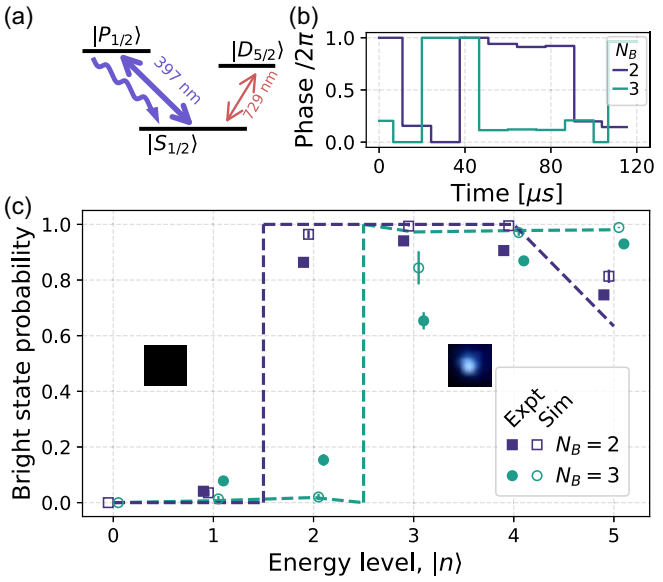


FIG. 2. (a) Simplified $^{40}Ca^+$ level diagram. Internal state detection is performed using the dipole-allowed 397 nm transition, which scatters photons rapidly if in the $|S_{1/2}\rangle$ state, and is dark if in the $|D_{5/2}\rangle$ state. The composite-phase pulse sequence is done on the quadrupole 729 nm transition, which hosts the internal qubit. (b) Composite laser pulse sequence for $N_B = 2, 3$. (c) Steplike excitation profile of the composite phase pulses with thresholds $N_B = 2, 3$. The dashed lines are the simulated profile of the step pulse sequence. The solid points are the experimental results, with 1σ error bars. The empty points show the simulated mean excitation (with 1σ error) given the measured Rabi frequency noise. For many points, the error bars are are too small to be seen. We perform about 400 experimental trials for each point. See Supplemental Material [58] for detailed error analysis. We show pictures of the single ion when in the dark state on the left, and in the bright state on the right.

support their possible implementation [36,44,46,47]. For example, by using the methods developed here, so-called concurrent measurements that can check the outcome of a quantum walk search while preserving the relevant quantum coherences may be implemented. We also expect that QFPTDs can be used for precision measurement as repeatedly monitored quantum systems offer sensing advantages, notably through quantum hindsight effects [48–50].

Trapped atomic ions are an ideal platform for experimental QFPTD measurements. Their prominence in quantum information processing has led to the development of a variety of coherent [51] and incoherent [52] control techniques that can be leveraged to simulate a broad variety of QFPTDs. Furthermore, by coupling the ion to different engineered reservoirs, variations of our QFPTD measurement technique can be used to test dynamical emergence [53]. In this Letter, we measure QFPTDs of a motional degree of freedom of a trapped ion driven by electric-field noise. We develop a widely applicable projective measurement protocol to measure whether or not an energy threshold is exceeded. We measure QFPTDs for various energy barriers and measurement intervals, and find agreement with theoretical predictions.

Projective measurement protocol. The *surviving* domain is defined in terms of the energy eigenstates $|n\rangle$ of the unperturbed oscillator: $\{|0\rangle, |1\rangle, |2\rangle, \ldots, |N_B - 1\rangle\}$. We define a projective measurement with two possible outcomes ("survival" and "absorption"), whose projectors $\mathbb{P}^{\mathrm{S}} = \sum_{n=0}^{N_B-1} |n\rangle\langle n|$ and $\mathbb{P}^{\mathrm{A}} = \sum_{n=N_B}^{\infty} |n\rangle\langle n|$ correspond to the *surviving* and *absorbing* domains, respectively. We dub the measurement "step pulse" as it effectively forms a quantum low-pass filter for the energy eigenstates. In order to implement this measurement on a trapped $^{40}Ca^+$ ion, whose internal states are shown in Fig. 2(a), we use a composite-phase laser pulse sequence shown in Fig. 2(b). Composite pulses, first used in nuclear magnetic resonance (NMR) spectroscopy, have been used in a variety of contexts to cancel errors (such as the famous Solovay-Kitaev SK1 and Wimperis broadband BB1 sequences [54–56]), and more recently to detect occupation of harmonic oscillator states [57]. Detuning a 729 nm laser by the motional frequency above the $|S_{1/2}\rangle \leftrightarrow |D_{5/2}\rangle$ transition gives rise to an anti-Jaynes-Cummings Hamiltonian. This interaction, known as the first blue sideband (BSB), couples the $|S_{1/2}\rangle \otimes |n\rangle$ and $|D_{5/2}\rangle \otimes |n+1\rangle$ states with n-dependent coupling strength [51]. We exploit the coupling-strength dependence on n to perform an effective π pulse on the internal state for $|n \geqslant N_B\rangle$ (leaving the internal state unaffected for $|n < N_B\rangle$) using a series of BSB pulses of different relative phases and durations, which we find using numerical optimization. We show a plot of the expected excitation probability as a function of the motional quantum number for different barriers in Fig. 2(c), from which the steplike nature of the pulse is clear. A subsequent projective measurement of the internal state completes the implementation of the projective motional state measurement.

In principle, with pulses of sufficient duration and complexity, this conditional excitation can be performed with near-unit fidelity. However, due to the limited coherence time of the ion and control errors, there is, in practice, a trade-off between the increase in fidelity gained by increasing the duration (and complexity) of the composite pulse and the effects of decoherence that get worse with increasing time. See Supplemental Material [58] for more details on the step pulse and these trade-offs.

In order to measure a QFPTD, we perform repeated trials and aggregate the first-passage times. For stroboscopic measurements with fixed interval θ, and where $P^{\mathrm{S(A)}}(i\theta)$ is the probability of obtaining a *survival* (*absorption*) outcome from the ith measurement given that all prior measurements resulted in *survival*, the QFPTD is given by

$$P^{\mathrm{FPT}}(k\theta) = \prod_{i=1}^{k-1} P^{\mathrm{S}}(i\theta) \times P^{\mathrm{A}}(k\theta). \tag{1}$$

The first passage occurs when the first *absorption* measurement is obtained. Thus, a single trial proceeds as follows: The ion is ground state cooled using resolved-sideband cooling [51], and the internal state is optically pumped to $|D_{5/2}\rangle$. Thus, each trial starts with the ion in

$$|\psi(t=0)\rangle = |D_{5/2}\rangle \otimes |0\rangle\,. \tag{2}$$

Then, in the quantum trajectories picture, the noisy electric field $\xi(t)$ causes a motional wavefunction $|\psi(t)\rangle$ to evolve for a time θ according to $|\psi(t)\rangle \to |\psi(t+\theta)\rangle = [I \otimes \mathcal{D}(\alpha)]\,|\psi(t)\rangle$, where $\alpha = ie/(\sqrt{2m\omega\hbar}) \int_t^{t+\theta} dt' \xi(t') e^{i\omega t'}$ and where $\mathcal{D}(\alpha)$ is the displacement operator [59,60]. Thus, in the absence of measurements, an initially coherent state is expected to remain coherent under the influence of the noise. Therefore, before the first measurement, the wavefunction is

$$|\psi(\theta^-)\rangle = |D_{5/2}\rangle \otimes \left(\sum_{n=0}^{\infty} d_n(\theta)\,|n\rangle\right), \tag{3}$$

where d_n are the coefficients of the randomly displaced motional wavefunction. We then apply the composite-phase pulse with the 729 nm laser that flips the internal state if the motional state is $|n \geqslant N_B\rangle$, and leaves the internal state unaffected if the motional state is $|n < N_B\rangle$:

$$|\psi(\theta^+)\rangle = |D_{5/2}\rangle \otimes \left(\sum_{n=0}^{N_B-1} d_n(\theta)\,|n\rangle\right) + |S_{1/2}\rangle \otimes \left(\sum_{N_B}^{\infty} d_n(\theta)\,|n\rangle\right). \tag{4}$$

After the composite pulse, the ion is in an entangled state between internal energy levels and the motion. A subsequent measurement of the ion internal state using state-dependent resonance fluorescence at 397 nm has two possible outcomes [Fig. 2(a)]: $|S_{1/2}\rangle$ in which case the ion fluoresces and photons are rapidly emitted (so-called "bright" state), or it can collapse to the $|D_{5/2}\rangle$ state and emit no photons (so-called "dark" state). Camera images of the ion in both bright and dark states are shown in Fig. 2(c). This measurement of the internal state completes the measurement and projects the motional state either into the *surviving* or *absorbing* domain. If a *survival* outcome is obtained, the ion is in state

$$|\psi(\theta^+)\rangle_{\mathrm{Survival}} = |D_{5/2}\rangle \otimes \left(\frac{1}{\sqrt{P^{\mathrm{S}}(\theta)}} \sum_{n=0}^{N_B-1} d_n(\theta)\,|n\rangle\right), \tag{5}$$

and the trial continues for another time interval θ and the step pulse is reapplied. This sequence is repeated until a bright measurement is obtained, after which the trial is terminated. We designed this measurement technique such that in the case that a dark state is obtained, a faithful quantum projective measurement has occurred. However, if a bright state is obtained, the motional state is altered due to to photon recoil. This has no impact on the FPTD since the trial is ended at that point. These types of two-step measurement protocols where a first "logic" pulse maps the motional state onto the internal state that is subsequently projectively measured are known to produce faithful quantum measurements of the motional state in the case that a dark outcome is obtained [61].

QFPTD predictions. Having established the QFPTD experimental protocol, we now present a few theoretical predictions. In this experiment, the ion is coupled to the natural, high-temperature amplitude reservoir from noisy electric fields in the environment [52]. This electric-field noise causes an initially ground-state cooled ion to heat and evolve to a thermal state of average occupation number $\bar{n}$. We independently measure the heating rate $\dot{\bar{n}}$ at the motional frequency ω through the standard sideband asymmetry technique. We then relate the heating rate to the noise spectral density using $\dot{\bar{n}}(\omega) = (e^2/4m\omega\hbar) S_\xi(\omega)$ [62]. We note that, in quantum mechanics, we distinguish between closed systems, which evolve unitarily, and open systems, which do not. The QFPTD measurement scheme developed in this Letter can be used in both cases.

The evolution of the motional state due to the electric-field noise in between measurements can be described using either quantum trajectory theory or a quantum master equation. For the density matrix ρ, the master equation is [52]

$$\dot{\rho} = \frac{\dot{\bar{n}}}{2}(2a\rho a^\dagger - a^\dagger a\rho - \rho a^\dagger a + 2a^\dagger \rho a - aa^\dagger \rho - \rho aa^\dagger), \tag{6}$$

where $a^\dagger(a)$ is the motional state creation (annihilation) operator. We also write Eq. (6) as $\dot{\rho} = \mathcal{M}\rho$. This evolution closely resembles a well-known classical analog: the classical undamped harmonic oscillator driven by additive noise, $\ddot{x} + \omega^2 x = e\xi(t)/m$, where m is the mass of the ion [63–65]. For convenience, we henceforth adopt dimensionless time t, such that $\dot{\bar{n}} = 1$, and use the independently measured value of $\dot{\bar{n}}$ to relate experimental and theoretical timescales. The normalized density matrix representing the surviving states immediately after the nth measurement at $t = n\theta$ is given by a renewal equation

$$\rho(t = n\theta^+)_{\mathrm{Surviving}} = \frac{[\mathbb{P}^{\mathrm{S}} e^{\theta\mathcal{M}}]^n \rho(t=0) [\mathbb{P}^{\mathrm{S}}]^n}{P^S(\theta) P^S(2\theta) \cdots P^S(n\theta)}, \tag{7}$$

from which the QFPTD is calculated. The diffusion along the energy ladder is then due to both the noisy evolution and quantum projection noise. Furthermore, we note that Eq. (6) may admit nonclassical initial conditions [63], and due to the projective measurements, the surviving states in Eq. (7)

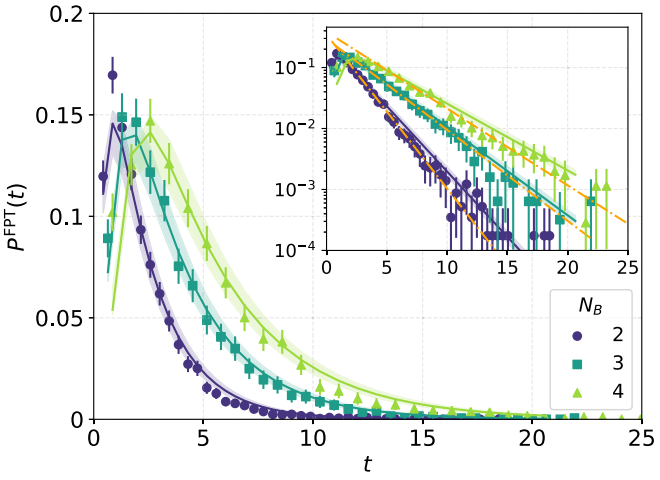


FIG. 3. Experimentally measured QFPTDs for $N_B = 2, 3, 4$ with intervals $\theta = 0.43, 0.645, 0.86$ (corresponding to 5, 7.5, and 10 ms, respectively), and with 6900, 3650, and 4250 trials, respectively. The points (with 1σ error bars) are data and the corresponding lines represent theoretical predictions of our model obtained by numerically solving Eqs. (1) and (7). See Supplemental Material [58] for more details on error analysis. The shaded error region around the lines represents the 1σ uncertainty of the measured heating $\dot{\bar{n}}$. The x axis is dimensionless time t, which is related to real time t' by $t = \dot{\bar{n}}t'$. In the inset, the same data are shown with overlaid orange dashed lines, which are fits of the measured distribution tails to an exponential.

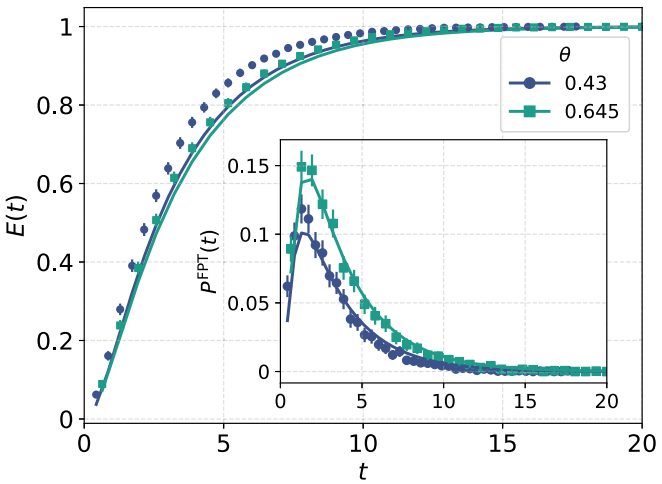


FIG. 4. Escape probability $E(t)$ and QFPTD $P^{\mathrm{FPT}}(t)$ (inset) for $N_B = 3$ with $\theta = 0.43, 0.645$, and with 3800 and 3650 trials, respectively. The experimental data are shown using the scattered points, and the theoretical predictions are shown using solid lines. The error bars represent 1σ uncertainties. For the escape probability, they reflect the negative covariance between the probability estimators in the QFPTD, as the underlying statistics follow a multinomial distribution. See Supplemental Material [58] for details on error bars.

become nonclassical [66]. We numerically solve Eq. (7) to obtain the QFPTD and show the results in Fig. 3 along side the experimental results. For finite θ, we predict a reduction of the mean first-passage time for decreasing θ. This effect is reflected in the escape probability $E(t;\theta) = \sum_{i=1}^{t/\theta} P^{\mathrm{FPT}}(i\theta)$ at time t, which is larger for smaller θ: i.e., $E(t;\theta_1) < E(t;\theta_2)$ if $\theta_1 > \theta_2$. This enhancement is shown in the theoretically predicted curves in Fig. 4. Although it appears to be an anti-Zeno effect, the enhancement of the escape probability arises because faster probing detects an escape sooner. This process is analogous to evaporative cooling of atom clouds [in particular to the radio-frequency (RF) knife technique [67]], where in this case, surviving trajectories have lower average energy than if nonselective measurements had been performed. Furthermore, due to the nonclassical quantization of energy, for $N_B = 1$ the QFPTD is a pure exponential (shown in the Supplemental Material [58]) without an initial ballistic part seen for $N_B \geqslant 2$, as each measurement resulting in survival projects the motional state back into $|0\rangle$, and thus the first-passage process follows a geometric distribution as the probability of measuring an escape is fixed. This is described in the Suppplemental Material [58].

Experimental results. We perform these experiments in a cryogenic linear Paul trap whose heating rate, measured by sideband asymmetry, is $\dot{\bar{n}} = 86 \pm 8$ q/s. We use a radial mode with Lamb-Dicke parameter $\eta = 0.055$ and carrier Rabi frequency $\Omega_{00} \sim 2\pi \times 300$ kHz. We validate the selective excitation profile of the step pulse by creating number states of motion $|n\rangle$, applying the step pulse, and then measuring the internal state excitation probability. The number states are created by first ground-state cooling the ion to $|S, 0\rangle$ and then using a sequence of BSB π pulses of the appropriate duration [51]. The results of the test and the expected excitation profile are shown in Fig. 2(c). The overwhelming majority of the errors in the step pulse measurement sequence come from the composite-phase pulse, and not the subsequent state-dependent fluorescence, which is performed with error $<10^{-3}$. We mainly attribute errors in the step pulse to laser intensity noise caused by vibrations from the cryostat motor in the experimental assembly, leading to beam-pointing instability. This causes the Rabi frequency to drift and fluctuate. See Supplemental Material [58] for a more detailed analysis of the Rabi frequency noise. In Fig. 2(c), we show simulated results with Rabi frequency noise (estimated from independent measurements) alongside experimental data. We also have contributions from imperfect ground state cooling (which results in lower number state creation fidelity), and smaller contributions from internal state decoherence ($T_2 \sim 580$ μs) due to slow B-field fluctuations, and motional state decoherence ($T_2 \sim 280$ μs). See Supplemental Material [58] for a more detailed error analysis and for details of the setup and control system.

Experimental QFPTD measurement results for $N_B = 2, 3, 4$ are shown in Fig. 3. The experimental results—notably their long-time behavior—show good agreement with the theoretical predictions and are consistent with an exponential decay at long times. As N_B increases, the ballistic portion is longer, in good agreement with theory. Pulse errors tend to increase the probability of early detection, thereby shifting the QFPTD forward in time. This effect also contributes to an exponential tail with a shorter characteristic time than that of the corresponding theoretical prediction. In order to compare the effect of moving N_B without becoming dominated by step pulse errors, in Fig. 3 we scale θ proportionally to N_B.

In a separate experiment, we explore a critical aspect of stroboscopic QFPTDs: the dependence of the escape probability on θ. We compare QFPTDs with $N_B = 3$ and different θ in Fig. 4. Since the QFPTDs shown here are probabilities and not probability densities, direct comparison of the QFPTDs for different values of θ is done using the escape probability. The experimental results are consistent with the presence of an enhancement of the escape probability for smaller θ. However, with current step pulse error rates, these data do not conclusively demonstrate it. This enhancement is a consequence of the repeated measurements within each run that modify the trajectory. If instead measurements were performed once in a run, then an "escape" probability could be reconstructed, but it would be insensitive to θ.

We have tacitly assumed that there is no spontaneous emission of the $|D_{5/2}\rangle$ state (lifetime 1.2 s [68]) between stroboscopic measurements. The duration of these experiments is sufficiently short that errors due to spontaneous emission do not dominate. While this poses a limitation to directly measuring QFPTDs that go out to long times, this problem can be circumvented by using either longer-lived optical qubits, such as barium [69], or ground-state qubits with practically infinite lifetimes [70]. Furthermore, given knowledge of the excited state lifetime, the true QFPTD can be reconstructed from the observed QFPTD that has been modified by spontaneous emission.

Conclusions. We develop and validate a way to use the motion of a trapped ion to measure QFPTDs. We use this method to measure experimentally the QFPTD of the ion energy when it is coupled to a high-temperature amplitude reservoir and show good agreement with theory. The step pulse measurements developed here can potentially be used for bosonic state engineering and simulation [71,72]. Further engineering of bespoke measurement operators raises the possibility of studying the properties of QFPTDs with more exotic surviving domains, such as quantum recurrence times [73] and winding numbers [74,75]. Complex interaction graphs for applications such as quantum walk search algorithms can be implemented using more cotrapped ions, thereby increasing the number of motional and spin degrees of freedom [71,76,77]. Using more trapped ions, the role of entanglement in QFPTDs could be investigated, which remains largely unexplored.

Acknowledgments. We are grateful to Jude Alnas for assistance with ARTIQ control. This work was funded by National Science Foundation under QLCI: Center for Robust Quantum Simulation Grant No. OMA-2120757. J.M.R. was supported by the Goshaw Fellowship. This manuscript was edited in part at the Aspen Center for Physics, which is supported by National Science Foundation Grant No. PHY-2210452.

Data availability. The data that support the findings of this article are openly available [78].

[1] C. Zunke, J. Bewerunge, F. Platten, S. U. Egelhaaf, and A. Godec, First-passage statistics of colloids on fractals: Theory and experimental realization, Sci. Adv. **8**, eabk0627 (2022).

[2] A. L. Thorneywork, J. Gladrow, Y. Qing, M. Rico-Pasto, F. Ritort, H. Bayley, A. B. Kolomeisky, and U. F. Keyser, Direct detection of molecular intermediates from first-passage times, Sci. Adv. **6**, eaaz4642 (2020).

[3] S. Redner, *A Guide to First-Passage Processes* (Cambridge University Press, Cambridge, 2001).

[4] E. Schrödinger, Zur theorie der fall-und steigversuche an teilchen mit brownscher bewegung, Phys. Z. **16**, 289 (1915).

[5] P. Hänggi, P. Talkner, and M. Borkovec, Reaction-rate theory: Fifty years after Kramers, Rev. Mod. Phys. **62**, 251 (1990).

[6] O. Bénichou, M. Moreau, and G. Oshanin, Kinetics of stochastically gated diffusion-limited reactions and geometry of random walk trajectories, Phys. Rev. E **61**, 3388 (2000).

[7] W. Dai, A. M. Sengupta, and R. M. Levy, First passage times, lifetimes, and relaxation times of unfolded proteins, Phys. Rev. Lett. **115**, 048101 (2015).

[8] M. A. Micheelsen, C. Rischel, J. Ferkinghoff-Borg, R. Guerois, and L. Serrano, Mean first-passage time analysis reveals rate-limiting steps, parallel pathways and dead ends in a simple model of protein folding, Europhys. Lett. **61**, 561 (2003).

[9] Y. Bomze, R. Hey, H. T. Grahn, and S. W. Teitsworth, Noise-induced current switching in semiconductor superlattices: Observation of nonexponential kinetics in a high-dimensional system, Phys. Rev. Lett. **109**, 026801 (2012).

[10] S. W. Teitsworth, M. E. Olson, and Y. Bomze, Scaling properties of noise-induced switching in a bistable tunnel diode circuit, Eur. Phys. J. B **92**, 74 (2019).

[11] N. Sazuka, J. ichi Inoue, and E. Scalas, The distribution of first-passage times and durations in forex and future markets, Phys. A: Stat. Mech. Appl. **388**, 2839 (2009).

[12] J. Perelló, M. Gutiérrez-Roig, and J. Masoliver, Scaling properties and universality of first-passage-time probabilities in financial markets, Phys. Rev. E **84**, 066110 (2011).

[13] R. Metzler, G. Oshanin, and S. Redner, *First-Passage Phenomena and Their Applications* (World Scientific, Singapore, 2014).

[14] C. Yin, Y. Wen, Z. Zong, and Y. Shen, The first passage time problem for mixed-exponential jump processes with applications in insurance and finance, Abstr. Appl. Anal. **2014**, 571724 (2014).

[15] S. N. Stechmann and J. D. Neelin, First-passage-time prototypes for precipitation statistics, J. Atmos. Sci. **71**, 3269 (2014).

[16] D. Lucente, C. Herbert, and F. Bouchet, Committor functions for climate phenomena at the predictability margin: The example of El Niño–southern oscillation in the Jin and Timmermann model, J. Atmos. Sci. **79**, 2387 (2022).

[17] D. Tesfay, L. Serdukova, Y. Zheng, P. Wei, J. Duan, and J. Kurths, Influence of extreme events modeled by Lévy flight on atlantic meridional overturning circulation stability, Phys. D: Nonlinear Phenom. **481**, 134849 (2025).

[18] K. Mølmer, Y. Castin, and J. Dalibard, Monte Carlo wavefunction method in quantum optics, J. Opt. Soc. Am. B **10**, 524 (1993).

[19] S. Maniscalco, J. Piilo, and K.-A. Suominen, Zeno and anti-Zeno effects for quantum Brownian motion, Phys. Rev. Lett. **97**, 130402 (2006).

[20] P. Hanggi and P. Talkner, First-passage time problems for non-Markovian processes, Phys. Rev. A **32**, 1934 (1985).

[21] F. Thiel, E. Barkai, and D. A. Kessler, First detected arrival of a quantum walker on an infinite line, Phys. Rev. Lett. **120**, 040502 (2018).

[22] D. A. Kessler, E. Barkai, and K. Ziegler, First-detection time of a quantum state under random probing, Phys. Rev. A **103**, 022222 (2021).

[23] M. J. Kewming, A. Kiely, S. Campbell, and G. T. Landi, First passage times for continuous quantum measurement currents, Phys. Rev. A **109**, L050202 (2024).

[24] H. Friedman, D. A. Kessler, and E. Barkai, Quantum walks: The first detected passage time problem, Phys. Rev. E **95**, 032141 (2017).

[25] E. H. Hauge and J. A. Støvneng, Tunneling times: A critical review, Rev. Mod. Phys. **61**, 917 (1989).

[26] J. Muga and C. Leavens, Arrival time in quantum mechanics, Phys. Rep. **338**, 353 (2000).

[27] S. Das and D. Dürr, Arrival time distributions of spin-1/2 particles, Sci. Rep. **9**, 2242 (2019).

[28] S. Das, M. Nöth, and D. Dürr, Exotic Bohmian arrival times of spin-1/2 particles: An analytical treatment, Phys. Rev. A **99**, 052124 (2019).

[29] S. Das and W. Struyve, Questioning the adequacy of certain quantum arrival-time distributions, Phys. Rev. A **104**, 042214 (2021).

[30] S. E. Venegas-Andraca, Quantum walks: A comprehensive review, Quantum Info. Proc. **11**, 1015 (2012).

[31] N. Shenvi, J. Kempe, and K. B. Whaley, Quantum random-walk search algorithm, Phys. Rev. A **67**, 052307 (2003).

[32] A. M. Childs and J. Goldstone, Spatial search by quantum walk, Phys. Rev. A **70**, 022314 (2004).

[33] D. Lewis, A. Benhemou, N. Feinstein, L. Banchi, and S. Bose, Optimal quantum spatial search with one-dimensional long-range interactions, Phys. Rev. Lett. **126**, 240502 (2021).

[34] D. Qu, S. Marsh, K. Wang, L. Xiao, J. Wang, and P. Xue, Deterministic search on star graphs via quantum walks, Phys. Rev. Lett. **128**, 050501 (2022).

[35] T. Yamasaki, H. Kobayashi, and H. Imai, Analysis of absorbing times of quantum walks, Phys. Rev. A **68**, 012302 (2003).

[36] J. Kempe, Discrete quantum walks hit exponentially faster, Probab. Theory Relat. Fields **133**, 215 (2005).

[37] R. Yin and E. Barkai, Restart expedites quantum walk hitting times, Phys. Rev. Lett. **130**, 050802 (2023).

[38] F. Thiel, I. Mualem, D. Meidan, E. Barkai, and D. A. Kessler, Dark states of quantum search cause imperfect detection, Phys. Rev. Res. **2**, 043107 (2020).

[39] Q. Liu, K. Ziegler, D. A. Kessler, and E. Barkai, Driving quantum systems with periodic conditional measurements, Phys. Rev. Res. **4**, 023129 (2022).

[40] S. Dhar, S. Dasgupta, A. Dhar, and D. Sen, Detection of a quantum particle on a lattice under repeated projective measurements, Phys. Rev. A **91**, 062115 (2015).

[41] S. Dhar, S. Dasgupta, and A. Dhar, Quantum time of arrival distribution in a simple lattice model, J. Phys. A: Math. Theor. **48**, 115304 (2015).

[42] H. Krovi and T. A. Brun, Quantum walks with infinite hitting times, Phys. Rev. A **74**, 042334 (2006).

[43] N. S. Williams and A. N. Jordan, Entanglement genesis under continuous parity measurement, Phys. Rev. A **78**, 062322 (2008).

[44] S. Tornow and K. Ziegler, Measurement-induced quantum walks on an IBM quantum computer, Phys. Rev. Res. **5**, 033089 (2023).

[45] B. Walter, G. Perfetto, and A. Gambassi, Thermodynamic phases in first detected return times of quantum many-body systems, Phys. Rev. A **111**, L040202 (2025).

[46] Q. Wang, S. Ren, R. Yin, K. Ziegler, E. Barkai, and S. Tornow, First hitting times on a quantum computer: Tracking vs. local monitoring, topological effects, and dark states, Entropy **26**, 869 (2024).

[47] R. Yin, Q. Wang, S. Tornow, and E. Barkai, Restart uncertainty relation for monitored quantum dynamics, Proc. Natl. Acad. Sci. USA **122**, e2402912121 (2025).

[48] S. Gammelmark, B. Julsgaard, and K. Mølmer, Past quantum states of a monitored system, Phys. Rev. Lett. **111**, 160401 (2013).

[49] D. Tan, S. J. Weber, I. Siddiqi, K. Mølmer, and K. W. Murch, Prediction and retrodiction for a continuously monitored superconducting qubit, Phys. Rev. Lett. **114**, 090403 (2015).

[50] M. Tsang, Time-symmetric quantum theory of smoothing, Phys. Rev. Lett. **102**, 250403 (2009).

[51] D. Leibfried, R. Blatt, C. Monroe, and D. Wineland, Quantum dynamics of single trapped ions, Rev. Mod. Phys. **75**, 281 (2003).

[52] Q. A. Turchette, C. J. Myatt, B. E. King, C. A. Sackett, D. Kielpinski, W. M. Itano, C. Monroe, and D. J. Wineland, Decoherence and decay of motional quantum states of a trapped atom coupled to engineered reservoirs, Phys. Rev. A **62**, 053807 (2000).

[53] Y. Ashida, Z. Gong, and M. Ueda, Non-Hermitian physics, Adv. Phys. **69**, 249 (2020).

[54] K. R. Brown, A. W. Harrow, and I. L. Chuang, Arbitrarily accurate composite pulse sequences, Phys. Rev. A **70**, 052318 (2004).

[55] S. Wimperis, Iterative schemes for phase-distortionless composite 180° pulses, J. Magn. Reson. **93**, 199 (1991).

[56] S. Wimperis, Broadband, narrowband, and passband composite pulses for use in advanced NMR experiments, J. Magn. Reson. Ser. A **109**, 221 (1994).

[57] M. Mallweger, M. Guevara-Bertsch, B. T. Torosov, R. Thomm, N. Kuk, H. Parke, C. F. Roos, G. Higgins, M. Hennrich, and N. V. Vitanov, Motional-state analysis of a trapped ion by ultranarrowband composite pulses, Phys. Rev. A **110**, 053103 (2024).

[58] See Supplemental Material at http://link.aps.org/supplemental/10.1103/p3pl-1m6n for details on the experimental setup, composite-phase step pulse sequence, laser intensity noise models, sampling error bars, and the qualitative difference between QFPTDs with $N_B = 1$ and $N_B \geqslant 2$, which includes Refs. [51,79,80].

[59] D. F. V. James, Theory of heating of the quantum ground state of trapped ions, Phys. Rev. Lett. **81**, 317 (1998).

[60] A. J. Rasmusson, I. Jung, F. Schroer, A. Kyprianidis, and P. Richerme, Measurement-induced heating of trapped ions, J. Phys. B: At. Mol. Opt. Phys. **57**, 225002 (2024).

[61] C. Flühmann, T. L. Nguyen, M. Marinelli, V. Negnevitsky, K. Mehta, and J. P. Home, Encoding a qubit in a trapped-ion mechanical oscillator, Nature (London) **566**, 513 (2019).

[62] M. Brownnutt, M. Kumph, P. Rabl, and R. Blatt, Ion-trap measurements of electric-field noise near surfaces, Rev. Mod. Phys. **87**, 1419 (2015).

[63] C. W. Gardiner and P. Zoller, *Quantum Noise: A Handbook of Markovian and Non-Markovian Quantum Stochastic Methods with Applications to Quantum Optics*, 3rd ed., Springer Series in Synergetics (Springer, Berlin, Heidelberg, 2004).

[64] H.-P. Breuer and F. Petruccione, *The Theory of Open Quantum Systems* (Oxford University Press, Oxford, 2007).

[65] T. P. Harty, High-fidelity microwave-driven quantum logic in intermediate-field $^{43}Ca^{+}$, Ph.D. thesis, University of Oxford, 2013.

[66] J. M. Ryan, S. W. Teitsworth, and C. Noel (unpublished).

[67] W. Vassen, C. Cohen-Tannoudji, M. Leduc, D. Boiron, C. I. Westbrook, A. Truscott, K. Baldwin, G. Birkl, P. Cancio, and M. Trippenbach, Cold and trapped metastable noble gases, Rev. Mod. Phys. **84**, 175 (2012).

[68] A. Kreuter, C. Becher, G. P. T. Lancaster, A. B. Mundt, C. Russo, H. Häffner, C. Roos, J. Eschner, F. Schmidt-Kaler, and R. Blatt, Spontaneous emission lifetime of a single trapped Ca^{+} ion in a high finesse cavity, Phys. Rev. Lett. **92**, 203002 (2004).

[69] A. A. Madej and J. D. Sankey, Quantum jumps and the single trapped barium ion: Determination of collisional quenching rates for the $5d^2D_{5/2}$ level, Phys. Rev. A **41**, 2621 (1990).

[70] M. Kang, W. C. Campbell, and K. R. Brown, Quantum error correction with metastable states of trapped ions using erasure conversion, PRX Quantum **4**, 020358 (2023).

[71] O. Katz and C. Monroe, Programmable quantum simulations of bosonic systems with trapped ions, Phys. Rev. Lett. **131**, 033604 (2023).

[72] K. Sun, M. Kang, H. Nuomin, G. Schwartz, D. N. Beratan, K. R. Brown, and J. Kim, Quantum simulation of spin-boson models with structured bath, Nat. Commun. **16**, 4042 (2025).

[73] M. Štefaňák, I. Jex, and T. Kiss, Recurrence and Pólya number of quantum walks, Phys. Rev. Lett. **100**, 020501 (2008).

[74] Y.-J. Wang, R.-Y. Yin, L.-Y. Dou, A.-N. Zhang, and X.-B. Song, Quantum first detection of a quantum walker on a perturbed ring, Phys. Rev. Res. **5**, 013202 (2023).

[75] X.-Y. Xu, Q.-Q. Wang, W.-W. Pan, K. Sun, J.-S. Xu, G. Chen, J.-S. Tang, M. Gong, Y.-J. Han, C.-F. Li, and G.-C. Guo, Measuring the winding number in a large-scale chiral quantum walk, Phys. Rev. Lett. **120**, 260501 (2018).

[76] C. Monroe, W. C. Campbell, L.-M. Duan, Z.-X. Gong, A. V. Gorshkov, P. W. Hess, R. Islam, K. Kim, N. M. Linke, G. Pagano, P. Richerme, C. Senko, and N. Y. Yao, Programmable quantum simulations of spin systems with trapped ions, Rev. Mod. Phys. **93**, 025001 (2021).

[77] Y. Lu, W. Chen, S. Zhang, K. Zhang, J. Zhang, J.-N. Zhang, and K. Kim, Implementing arbitrary ising models with a trapped-ion quantum processor, Phys. Rev. Lett. **134**, 050602 (2025).

[78] J. M. Ryan, S. Gorbaty, T. J. Kessler, M. G. Peaks, S. W. Teitsworth, and C. Noel, Data from "Experimental measurement of quantum first-passage time distributions" [Dataset], Duke Research Data Repository (2025), https://doi.org/10.7924/R4HT2X079.

[79] P. Virtanen, R. Gommers, T. E. Oliphant, M. Haberland, T. Reddy, D. Cournapeau, E. Burovski, P. Peterson, W. Weckesser, J. Bright, *et al.*, SciPy 1.0: Fundamental algorithms for scientific computing in Python, Nat. Methods **17**, 261 (2020).

[80] G. Pagano, P. W. Hess, H. B. Kaplan, W. L. Tan, P. Richerme, P. Becker, A. Kyprianidis, J. Zhang, E. Birckelbaw, M. R. Hernandez, Y. Wu, and C. Monroe, Cryogenic trapped-ion system for large scale quantum simulation, Quantum Sci. Technol. **4**, 014004 (2018).